29th International Conference
ENGINEERING MECHANICS 2023
Milovy, Czech Republic, May 9 – 11, 2023

CONSISTENCY OF MATHEMATICAL AND EXPERIMENTAL MODEL OF THE AUTOPARAMETRIC SYSTEM

Fischer C.[*], **Náprstek J.**[**]

Abstract: *This paper presents a long-overdue comparison of data obtained from experimental investigation of a spherical vibration absorber with the results of two mathematical models of the motion of a heavy sphere in a spherical surface. It shows that the danger posed by the potentially unstable self-parametric nature of the mathematical system is not too great in the case of realistic configurations, and that the values of the parameters describing the realistic structures remain within intervals corresponding to the stable behaviour of the absorber.*

Keywords: Vibration absorber, Rolling sphere, Spherical surface, Autoparametric system, Structural health monitoring.

1. Introduction

Passive tuned mass vibration absorbers are well-established in engineering literature; see the exhaustive review paper by Elias and Matsagar (2017) or the recent one due to Yang et al. (2021). The *ball-type absorbers* use the rolling movement of a heavy sphere inside a spherical recess to reduce vibration of the connected structure. However, ball-type absorbers have limited adjustability of damping, making them more susceptible to objectionable effects resulting from the nonlinear character of the system. Dynamic stability analysis should be therefore a necessary part of the design process. Thus, it is surprising that Elias and Matsagar (2017) do not mention any text concerning the dynamic stability analysis of structures equipped with vibration absorbers.

This paper presents the synthesis that was lacking in previously published engineering and theoretical papers. It builds on the design, in-situ and experimental investigation published by (Pirner, 2002) and the theoretical models summarized by the authors in (Náprstek and Fischer, 2018).

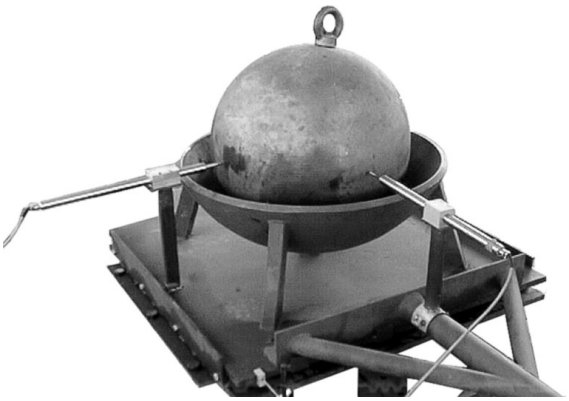

Fig. 1: Experimental setup

2. Description of the experiment

The spherical recess with a casted iron sphere was fastened to a table supported by nine steel balls enabling the excitation of its movement by one or two mutually perpendicular forces, see Fig. 1. The forces were supplied by one (uniaxial excitation) or two (biaxial excitation) MTS cylinders (jacks) via arms. The "position control" method was selected in which the excited movement displacement of the supporting plate was kept approximately constant; the excitation force was variable depending on excitation frequency. During each test, the excitation frequency was varied regularly within the range of 0.7 and 1.6 Hz in steps of 0.1 Hz and in the resonance domain in steps of 0.05 Hz. The duration of one step was 30 s and the transition time from one step to another was 15 s. The parameters of the examined absorber were: $m = 870$ kg, $R = 0.41$ m, $r = 0.3$ m.

[*,**] RNDr. Cyril Fischer, Ph.D., Ing. Jiří Náprstek, DrSc., Institute of Theoretical and Applied Mechanics, Prosecká 76, 190 00 Prague 9, tel. +420 225 443 221, e-mail {fischerc,naprstek}@itam.cas.cz

ISSN: 1805-8256, doi: 10.21495/em2023-67

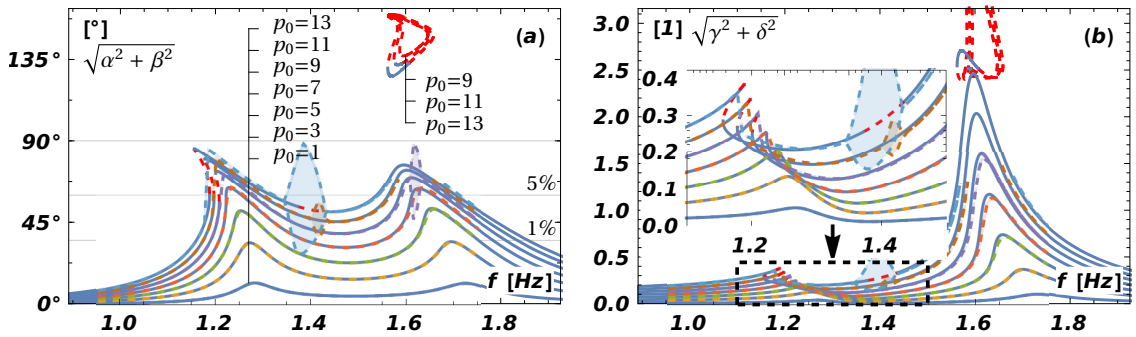

Fig. 2: Analytically and numerically obtained resonance curves for 2D mathematical model Eq. (1).

3. Matematical model in 2D

The Lagrangian model of the ball in a cavity, which is connected to a simple structure, is given as

$$\ddot{\varphi} + \kappa b_\varphi \dot{\varphi} + \kappa\omega_m^2 \sin\varphi + \kappa\ddot{\zeta}\cdot\cos\varphi = 0\,, \tag{1a}$$

$$\mu\ddot{\varphi}\cos\varphi - \mu\dot{\varphi}^2\sin\varphi + (1+\mu)\ddot{\zeta} + b_u\dot{\zeta} + \omega_M^2\zeta = p(t)\,, \tag{1b}$$

where $\mu = m/M$, $\omega_M^2 = C/M$, $\omega_m^2 = g/\varrho_r$, $\kappa = 5/7$, $\varrho_r = R-r$, $J = 2/5mr^2$, M, C are the mass and stiffness of the structure, b_u, b_φ are damping coefficients of the structure and absorber, respectively. The symbols φ, ζ describe deflection of the position vector of the sphere from the vertical axis of the cavity and $\zeta = (R-r)u$, u denotes the displacement of the cavity. The structure is excited by force $P = p_0(R-r)M$.

In order to identify the stationary amplitudes, excitation and the response are written as

$$p(t) = p_0\sin(\omega t)\,, \quad \varphi(t) = \alpha\sin(\omega t) + \beta\cos(\omega t)\,, \quad \zeta(t) = \gamma\sin(\omega t) + \delta\cos(\omega t)\,. \tag{2}$$

After substitution Eqs (2) into Eqs (1) and substituting the $\sin\varphi$ and $\cos\varphi$ functions by two terms of the Taylor expansion, the harmonic balance procedure gives differential system for unknown amplitudes $\mathbf{Z} = (\alpha, \beta, \gamma, \delta)^T$, see (Náprstek and Fischer, 2018) for details

$$\mathbf{M}(\mathbf{Z})\dot{\mathbf{Z}} = \mathbf{F}(\mathbf{Z}). \tag{3}$$

The system (3) is meaningful if changes in amplitudes $\mathbf{Z}$ within one period $2\pi/\omega$ can be neglected. Then matrix $\mathbf{M}$ and right hand side vector $\mathbf{F}$ are ($B_0 = \alpha^2+\beta^2$, $B_x = B_0 + 2x^2$)

$$\mathbf{M} = \begin{pmatrix} 0 & -\omega & -\frac{1}{4}\alpha\beta\kappa\omega & \frac{1}{8}\kappa\omega B_\alpha \\ \omega & 0 & -\frac{1}{8}\kappa\omega B_\beta & \frac{1}{4}\alpha\beta\kappa\omega \\ -\frac{1}{8}\mu\omega B_\beta & \frac{1}{4}\alpha\beta\mu\omega & (\mu+1)\omega & 0 \\ -\frac{1}{4}\alpha\beta\mu\omega & \frac{1}{8}\mu\omega B_\alpha & 0 & -(\mu+1)\omega \end{pmatrix}\,, \tag{4}$$

$$\mathbf{F} = -\begin{pmatrix} \frac{1}{8}\kappa\left((B_0-8)\left(\gamma\omega^2 - \alpha\omega_m^2\right) + 2\alpha\omega^2\left(\alpha\gamma+\beta\delta\right) - 8\beta\omega b_\varphi\right) - \alpha\omega^2 \\ \frac{1}{8}\kappa\left((B_0-8)\left(\delta\omega^2 - \beta\omega_m^2\right) + 2\beta\omega^2\left(\alpha\gamma+\beta\delta\right) + 8\alpha\omega b_\varphi\right) - \beta\omega^2 \\ \frac{1}{8}\mu\left(\beta B_0\left(\frac{1}{6}B_0+1\right) - 8(\beta+\delta)\right)\omega^2 + \delta\left(\omega_M^2 - \omega^2\right) + \gamma\omega b_u \\ \frac{1}{8}\mu\left(\alpha B_0\left(\frac{1}{6}B_0+1\right) - 8(\alpha+\gamma)\right)\omega^2 + \gamma\left(\omega_M^2 - \omega^2\right) - \delta\omega b_u \qquad - p_0 \end{pmatrix}\,. \tag{5}$$

If the system response is to be stationary, the derivatives $\mathrm{d}\mathbf{Z}/\mathrm{d}t$ will vanish and Eq. (3) degenerates into $\mathbf{F}(\mathbf{Z}) = 0$. The solutions to this equation represent the possible stationary vibration amplitudes of individual components. However, the stability of these stationary solutions should be assessed using the Routh-Hurwitz conditions computed for the Jacobian of the complete right-hand side of the normal system

$$\mathrm{jac}\left(\mathbf{M}^{-1}\mathbf{F}\right)\,. \tag{6}$$

The possible instability of the stationary solution using the 2D model comes from the interaction between the motion of the sphere in the container and the motion of the structure. However, as shown in Fig. 2, the instability appears only at higher amplitudes of harmonic excitation, where the unstable stationary amplitudes are marked as red dashed curves. It is clear that at deflections above $\phi \approx 60°(35°)$, where the relative error of the $\cos(\phi)$ polynomial replacement exceeds 5% (1%), the identified instability may no longer reliably describe the physical phenomenon. But comparison with numerical integration (dashed colour lines in Fig. 2) shows a qualitative agreement even for amplitudes $60° < \phi < 90°$. In the figure, the

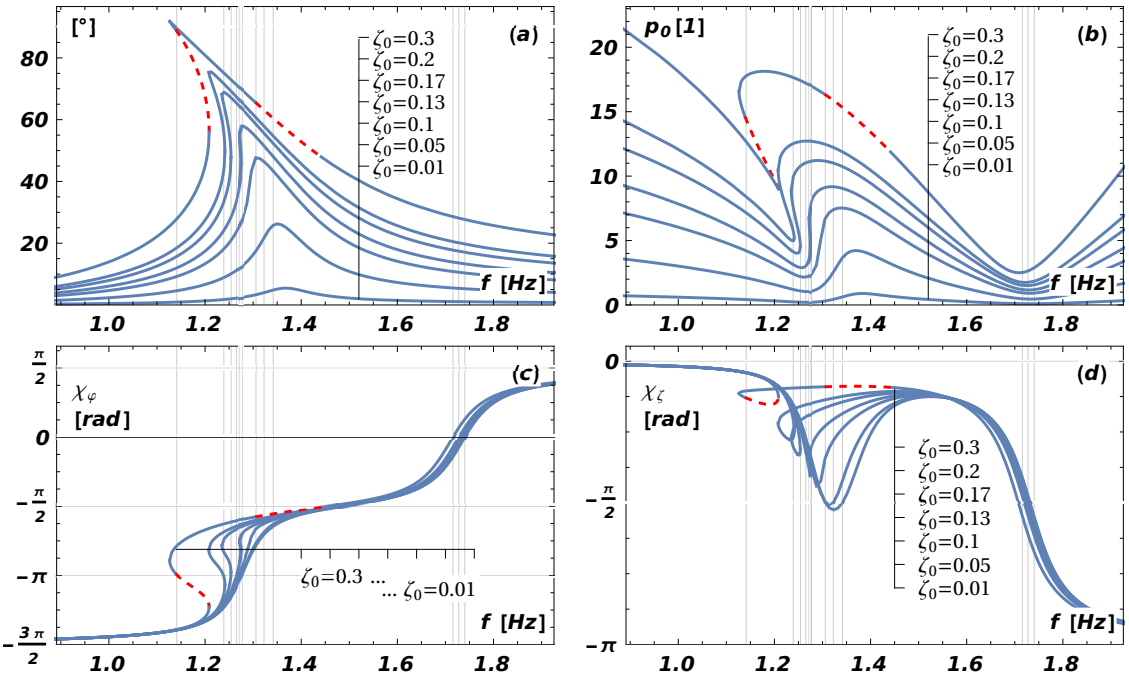

Fig. 3: Stationary amplitudes of the 2D model Eq. (1) for constant displacement amplitudes. Top: a) resonance curves for amplitudes of the sphere, b) forcing amplitudes necessary to obtain prescribed movement of the structure; bottom: phase shifts between forcing and movement of c) the sphere, d) the structure.

non-stationary response is indicated by the shaded area between the curves for the minimum and maximum values of the response amplitudes for a given constant excitation amplitude. It is worth noting that the curves for response amplitudes $\phi > 90°$ are no longer physically meaningful, but they make nice shapes.

In order to match the position control mechanism used during the experiment, Fig. 3 illustrates a case where the amplitude $|\zeta| = \sqrt{\gamma^2 + \delta^2}$ was prescribed constant while tracing the solutions of $\mathbf{F}(\mathbf{Z}) = 0$. Thus, the part corresponding to Eq. (1a) is a simple Duffing equation (plot (a) in Fig. 3), whereas the part representing the non-dimensional excitation force and interaction between the structure and the absorber (plot (b)) reveals two resonance regions. The resonance frequencies can be observed from the phase shift plots (c) and (d). It is important to note that only the lowest curve in the plot corresponds to the configuration of the experiment, with an amplitude of $|\zeta| = 0.014$, as shown in the experimental results in Fig. 4.

4. Mathematical model in 3D

Using a full 3D model allows for describing the instability of planar motion in the direction of harmonic excitation due to transverse perturbations. However, due to geometric constraints, assumptions such as harmonic character and small deflections of the response cannot be made in the 3D model. Despite the promising theoretical results of the authors in the case of undamped free motion of the sphere in the spherical recess, as presented in (Náprstek and Fischer, 2018), a numerical approach is required for the 3D case.

The 3D model is based on the derivation using the Appel-Gibbs approach published by Legeza (2002) and used by Náprstek and Fischer (2018). The original derivation contains a slight geometric inaccuracy, where the rotation of the sphere due to the curvature of the underlying the surface was not taken into account. The corrected governing system in Cartesian coordinates takes the form

$$\begin{aligned}
\dot{u}_{Cx} &= \frac{-r}{R-r}\left((R-u_{Cz})\omega_y + u_{Cy}\omega_z\right), & \dot{\omega}_x &= \frac{-1}{rR}\frac{5}{7}\left((R-u_{Cz})\ddot{u}_{Ay} + g\,u_{Cy}\right) - \frac{5}{7}b_\varphi\omega_x, \\
\dot{u}_{Cy} &= \frac{r}{R-r}\left((R-u_{Cz})\omega_x + u_{Cx}\omega_z\right), & \dot{\omega}_y &= \frac{1}{rR}\frac{5}{7}\left((R-u_{Cz})\ddot{u}_{Ax} + g\,u_{Cx}\right) - \frac{5}{7}b_\varphi\omega_y, \\
\dot{u}_{Cz} &= \frac{r}{R-r}\left(u_{Cy}\omega_x - u_{Cx}\omega_y\right), & \dot{\omega}_z &= \frac{1}{rR}\frac{5}{7}\left(u_{Cy}\ddot{u}_{Ax} - u_{Cx}\ddot{u}_{Ay}\right) - \frac{5}{7}b_\varphi\omega_z,
\end{aligned} \tag{7}$$

where u_{Cx}, u_{Cy}, u_{Cz} denote local coordinates of the contact point of the sphere within the spherical cavity, $\varphi_\bullet = R\sin(u_{C\bullet})$; $\omega_x, \omega_y, \omega_z$ are the angular velocities of the sphere with respect to local coordinate axes and u_{Ax}, u_{Ay} are movements of the cavity in the global coordinate system.

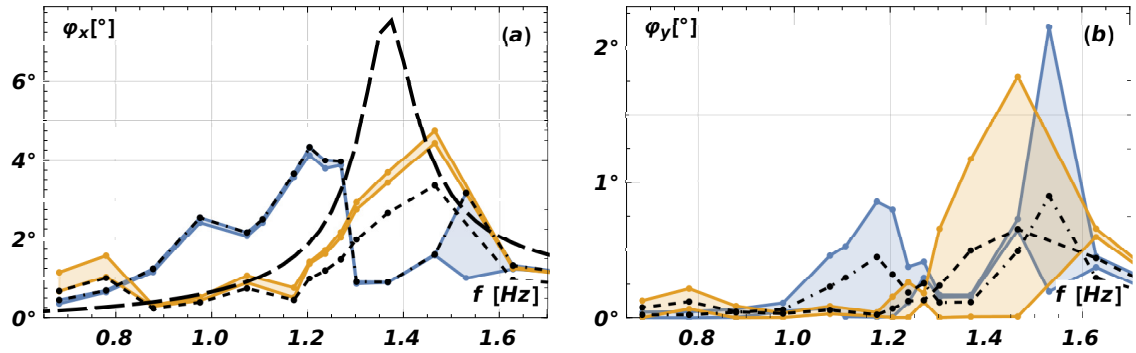

Fig. 4: Analytically (dashed line) and experimentally (segmented lines) obtained resonance curves for 3D mathematical model Eq. (7). a) longitudinal direction, b) transversal direction. The dot-dash line indicates the RMS values of the experimental values.

Figure 4 shows a comparison between the resonance curves obtained from experiments and numerical simulations. The experiments were carried out using a single excitation amplitude $\zeta_0 = 0.014$ and gradually increasing and decreasing frequency, resulting in blue and yellow solid polylines, respectively. The numerical simulations were based on Eq. (7) with $u_{Ax} = (R-r)\zeta_0 \cos(2\pi f t)$ and $u_{Ay} = 0$, also using $\zeta_0 = 0.014$. The numerical results are indicated by the black dashed line.

Graph (a) of Fig. 4 shows the motion in the excitation direction, while graph (b) shows the response in the transverse direction. The color-filled areas correspond to the region of the identified non-stationary response. The experiments were performed on a rubber-coated spherical cavity, resulting in a relatively large damping coefficient of $b_\varphi = 0.9$. Consequently, the mathematical model did not exhibit any stable transversal motion in plot (b) that was clearly present in the experiment. However, a qualitative match can be observed in graph (a), where the numerical and experimental results agree reasonably well.

5. Conclusions

This paper outlines a unified view of the theoretical, numerical, and experimental analysis of a nonlinear mechanical system. Both 2D and 3D theoretical models are presented, which describe the different instabilities that can occur in the motion of a sphere in a cavity. The stability analysis of stationary solutions of the 2D model is refined, and a corrected and simplified 3D model is presented. The experimental investigation is briefly mentioned due to space limitations.

Acknowledgments

The kind support of Czech Science Foundation project No. 21-32122J and of the RVO 68378297 institutional support are gratefully acknowledged.

References

Elias, S. and Matsagar, V. (2017) Research developments in vibration control of structures using passive tuned mass dampers. *Annu. Rev. Control*, 44, pp. 129–156.

Legeza, V. (2002) Determination of the amplitude-frequency characteristic of the new roller damper for forced oscillations. *J. Automat. Inform. Sci.*, 34, 5-8, pp. 32–39.

Náprstek, J. and Fischer, C. (2018) Appell-Gibbs approach in dynamics of non-holonomic systems. In Reyhanoglu, M., edt., *Nonlinear Systems*, IntechOpen, Rijeka, chapter 1, pp. 3–30.

Náprstek, J. and Fischer, C. (2021) Trajectories of a ball moving inside a spherical cavity using first integrals of the governing nonlinear system. *Nonlinear Dynamics*, 106, 3, pp. 1591–1625.

Pirner, M. (2002) Actual behaviour of a ball vibration absorber. *Journal of Wind Engineering and Industrial Aerodynamics*, 90, 8, pp. 987–1005.

Ren, Y. and Beards, C. F. (1994) A new receptance-based perturbative multi-harmonic balance method for the calculation of the steady state response of non-linear systems. *Journal of Sound and Vibration*, 172, 5, pp. 593–604.

Yang, F., Sedaghati, R., and Esmailzadeh, E. (2021) Vibration suppression of structures using tuned mass damper technology: A state-of-the-art review. *Journal of Vibration and Control*, 28, 7-8, pp. 812–836.